IEEE Access
Multidisciplinary | Rapid Review | Open Access Journal

Received April 21, 2021, accepted May 7, 2021, date of publication May 11, 2021, date of current version May 24, 2021.

Digital Object Identifier 10.1109/ACCESS.2021.3079332

A New Method of Insulation Detection on Electric Vehicles Based on a Variable Forgetting Factor Recursive Least Squares Algorithm

ZHENBIN CHEN[1], WEIYA CUI[1], XIANGYU CUI[2], HUIMIN QIAO[3], HAO LU[1], AND NA QIU[1]

[1]Mechanical and Electrical Engineering College, Hainan University, Haikou 570228, China
[2]Key Laboratory of Electrochemical Energy Storage and Energy Conversion of Hainan Province, College of Physics and Electronic Engineering, Hainan Normal University, Haikou 571158, China
[3]Haima Automobile Company Ltd., Zhengzhou 450000, China

Corresponding author: Xiangyu Cui (mymq0002@163.com)

This work was supported by the Finance Science and Technology Project of Hainan Province of China under Grant ZDYF2020032.

ABSTRACT The lithium-ion batteries of an electric vehicle belong to a high-voltage direct-current system. The high-voltage insulation performance of electric vehicles is very important for their safe operation. To solve the problems of slow response and the poor estimation accuracy of the insulation resistance under complex vehicle working conditions, a real-time insulation resistance detection method based on the variable forgetting factor least squares algorithm is proposed in this paper. Based on the low-frequency signal injection method and considering the influence of the Y capacitor, the corresponding circuit model and the mathematical model of the reflected wave voltage are established, and the mathematical model is linearized by a first-order Taylor expansion. By analyzing the influence of the forgetting factor on model parameter identification and setting appropriate shutdown criteria, the least squares algorithm with a variable forgetting factor is designed to quickly and accurately estimate the insulation resistance and Y capacitance. The experimental test results show that the proposed method can quickly track the changes in the insulation resistance and Y capacitance under the condition of noise interference and that the root mean square error of the estimation resistor is within 0.012.

INDEX TERMS Electric vehicle (EV), embedded micro-control unit, insulation detection, lithium-ion batteries, variable forgetting factor recursive least squares (VFFRLS).

NOMENCLATURE

ABBREVIATIONS

DC	direct current
EKF	extended Kalman filter
EV	electric vehicle
HVDC	high-voltage direct-current
MCU	micro-control unit
PC	personal computer
RC	resistor capacitor
RLS	recursive least squares
RMSE	root mean square error
UKF	unscented Kalman filter
VFFRLS	variable forgetting factor recursive least squares

SYMBOLS

a_1	Steady-state component of response
a_2	Response gain
a_3	Response time constant
$\widehat{a}_1(k-1)$	Estimated value of a_1 at time $k-1$
$\widehat{a}_2(k-1)$	Estimated value of a_2 at time $k-1$
$\widehat{a}_3(k-1)$	Estimated value of a_3 at time $k-1$
A	Parameters a_1, a_2, a_3
$\widehat{A}(k-1)$	Estimated values of parameters at time $k-1$
b	Scaling factor
C_n	Negative Y capacitance
C_p	Positive Y capacitance
$C_p//C_n$	Equivalent Y capacitance value
$\overline{C_p//C_n}$	Equivalent Y capacitance measurement result
$e(i)$	Difference between the observed value and the estimated value at time i
$E_{a_1}(k)$	Mean value of a_1 in the sliding window

The associate editor coordinating the review of this manuscript and approving it for publication was Wei Xu.

$E_{a_3}(k)$	Mean value of a_3 in the sliding window
H	Observation matrix
I_1	Current flowing through R_1
I_2	Current flowing through R_2
I_3	Current flowing through R_p
I_4	Current flowing through R_n
I_f	Current flowing through R_f
I_{f+}	Current flowing through R_f in the positive half period
J	Cost function
K	Gain of RLS
M	Maximum voltage value of the reflected wave
P	Error covariance matrix
Q	Root mean square noise value
R_1	Positive current limiting resistor
R_2	Negative current limiting resistor
R_f	Sampling resistor
R_n	Negative insulation resistance
$\overline{R_n}$	Negative insulation resistance measurement result
R_p	Positive insulation resistance
$\overline{R_p}$	Positive insulation resistance measurement result
U	Power battery voltage
U_f	Reflected wave voltage
U_{f+}	Reflected wave voltage in the positive half period
U_{f-}	Reflected wave voltage in the negative half period
U_{n0}	Initial voltage value of C_n
U_{p0}	Initial voltage value of C_p
U_s	Voltage value generated by the signal generator
U_{s+}	Voltage value generated by the signal generator in the positive half period
U_{s-}	Voltage value generated by the signal generator in the negative half period
V	One-dimensional random observation noise
Y	Constant error term
β	Parameter for calculating the forgetting factor
δ	Relative error
Δt	Sampling interval
λ	Forgetting factor
λ_0	Parameter for calculating the forgetting factor
λ_1	Parameter for calculating the forgetting factor
$\sigma_{a_1}(k)$	Standard deviation of a_1 in the sliding window
$\sigma_{a_3}(k)$	Standard deviation of a_3 in the sliding window

I. INTRODUCTION

As automobile pollutant emissions become increasingly serious [1], electric vehicles are becoming increasingly popular [2]–[6]. Lithium-ion batteries have high energy density and power density, and their high voltage can significantly improve the energy utilization efficiency. Therefore, most electric vehicles use high-voltage lithium-ion batteries as power batteries [7]–[9]. As the high-voltage lithium-ion battery belongs to high-voltage direct current (DC) systems, the high-voltage insulation performance of automobiles is of great significance for the safe driving of electric vehicles [10]–[12]. The operating conditions and operating environment of electric vehicles, including high temperature, high humidity, and high salt spray operating environments, are complex [13]–[18]. High-voltage electrical components exhibit high-voltage insulation changes or even high-voltage insulation failure. The China national standard file GB 18384-2020 [19] and the International Organization for Standardization standard file ISO 6469-1: 2019 [20] stipulated that the insulation resistance of the high voltage systems of electric vehicles must not be less than 100 V/ohm. Therefore, the real-time monitoring of electric vehicle high-voltage insulation performance changes and responding to the changes in the insulation resistance, represent important guarantees for the safe operation of electric vehicles. Because it is difficult to directly measure the high-voltage insulation of electric vehicles online, researchers have invented a variety of methods to detect the high-voltage insulation resistance [21]–[24], but most of them face problems such as a slow response time, insufficient estimation accuracy, and poor reliability. Therefore, it is necessary to study a new insulation resistance detection method with a rapid response, high estimation accuracy and high reliability.

A. REVIEW OF INSULATION RESISTANCE DETECTION APPROACHES

In the laboratory, a high-precision voltmeter is usually used to measure the voltage of the high-voltage direct-current (HVDC) system supplied to the electrical chassis in order to calculate the insulation resistance of the positive and negative poles of the HVDC system with respect to the automobile electrical chassis [19], [20]. This method requires a stopped electric vehicle for static testing, so it does not employ actual driving conditions to measure the insulation resistance of the HVDC system; therefore, the value of the promotion of the electric vehicle is not utilized. The balanced bridge method [25] has been the most commonly used high-voltage insulation resistance measurement method for electric vehicles due to its advantages of a simple measurement circuit and low cost. This method can accurately measure the insulation resistance of an HVDC system when the different insulation resistance value exists between the positive and negative poles of the HVDC system and the automobile electrical chassis. In the case of same insulation resistances, this method has an obvious measurement error, and in the case of high temperature and high humidity, the measurement error will be enhanced: the balanced bridge method has thus been eliminated by mainstream electric vehicle manufacturers. The unbalanced bridge method can overcome the shortcomings of the balanced bridge method but will greatly increase the cost of the measurement circuit. Additionally, this method cannot respond to the rapid change in the insulation resistance when the system has Y capacitance, so it is gradually replaced by other new methods in current electric vehicles.

In view of the influence of the Y capacitance on the measurement system, Mathsyaraja Aravind [26] proposed two new insulation resistance measurement methods. Method 1 designs the Y capacitor discharge circuit and uses the resistor capacitor (RC) characteristics of the HVDC system to estimate the insulation resistance of the system. This method can effectively measure the insulation resistance of the high voltage system when the Y capacitor is large enough, but when the Y capacitor is small, the discharge current is small, and the current measurement error will significantly affect the measurement result. Method 2 injects a high voltage into the HVDC system and calculates the insulation resistance of the HVDC system by observing the charging process of the Y capacitor. This method can quickly and accurately calculate the insulation resistance of the HVDC system but may cause damage to the HVDC systems of electric vehicles. Moreover, there is a risk that the measurement error will increase or even reach failure under the high frequency interference of the high voltage system. Due to its safety, reliability and low cost, the low-voltage and low-frequency voltage injection method to measure insulation resistance has gradually become the mainstream test method for the insulation resistance of the high voltage systems of electric vehicles [27]. The method injects a $\pm$ 34 V square wave with a frequency of 0.1 Hz into the high voltage system of electric vehicles, returns to the electric chassis after the voltage divider, and collects feedback from the electrical chassis. In addition, the Kalman filter algorithm [28] has been applied to filter noise, and the recursive least squares (RLS) algorithm [29] has been applied to solve the problem of the fluctuation of the insulation resistance detection results of a high voltage system caused by the unstable voltage of a power battery under complex working conditions. This method needs to calculate both the Kalman filter algorithm and RLS algorithm at the same time, which leads to an increase in computational complexity and the failure to run smoothly on a low-cost on-board microprocessor, which limits the application of this method in electric vehicles. Chuanxue Song [30] proposed an equivalent circuit model for HVDC insulation resistance measurements based on the method of low voltage and low-frequency voltage injection and used the extended Kalman filter (EKF) algorithm to estimate the insulation resistance of an HVDC system. This method can accurately estimate the insulation resistance of the HVDC system, but due to the large rounding error in the nonlinear process of the extended Kalman algorithm [31], the estimation of insulation resistance cannot be further improved. At the same time, in the case of strong noise interference, this method poses the problem of algorithm divergence [32].

B. CONTRIBUTIONS OF THIS STUDY

To overcome the problems of poor accuracy, slow response, low robustness and weak anti-interference ability of the above methods, based on the low-voltage low-frequency injection method, this paper analyzes the reflected wave, establishes a new insulation detection circuit model, and proposes the variable forgetting factor recursive least squares (VFFRLS) algorithm to estimate the insulation resistance of an HVDC system. Specifically, based on the low-frequency signal injection method, the influence of system Y capacitance is considered, the corresponding circuit model and the mathematical model of the reflected wave voltage are established, and the mathematical model is linearized by using a first-order Taylor expansion. By analyzing the influences of the forgetting factor on model parameter identification and setting appropriate shutdown criteria, the least squares algorithm with a variable forgetting factor is designed to quickly and accurately estimate the insulation resistance and Y capacitance values. This method has the advantages of a fast response speed (the average response time is 3 s), high robustness, high estimation accuracy (the root mean square error (RMSE) is less than 0.012) and strong anti-interference ability, which is suitable for promotion in electric vehicles.

C. ORGANIZATION OF THIS PAPER

The sections organized in the remainder of the paper are as follows: In Section 2, the calculation model of insulation resistance and the reflected wave voltage model affected by the Y capacitor are described. The VFFRLS algorithm for insulation resistance estimation is proposed in Section 3. Simulations and experimental configurations are presented in Section 4. Three experiments were performed on the simulation and test bench to verify the proposed method in Section 5. The main conclusions are drawn in Section 6.

II. MODEL DERIVATION BASED ON LOW-FREQUENCY SIGNAL INJECTION METHOD

A. INSULATION RESISTANCE CALCULATION MODEL

In this paper, when the circuit model for measuring insulation resistance by the low-frequency signal injection method is established, the power battery voltage is taken into account, and the calculation formula of the insulation resistance under the joint action of the pulse voltage and high voltage system is derived. Fig. 1 shows the insulation detection circuit model, in which the power battery voltage is U, the pulse signal generator is U_s, the equivalent insulation resistances of the positive and negative electrodes are R_p and R_n, the current limiting resistors of the detection equipment are R_1, R_2, and $R_1 = R_2 = R$, and the voltage at both ends of the sampling resistor R_f is U_f. The voltage values generated by the pulse signal generator in the positive and negative half periods are set as U_{s+} and U_{s-}, respectively.

In the positive half period, the pulse signal generator generates a step voltage with value U_{s+}, and the currents flowing on R_1, R_2, R_p, R_n, and R_f are I_1, I_2, I_3, I_4, and I_{f+}, respectively. U and R_p, R_n form loop II, U and R_1, R_2 form loop I, U_s and R_p, R_1, R_f form loop III. It is assumed that the power battery voltage remains constant within one pulse period. According to Kirchhoff's law:

$$I_{f+} = I_1 + I_2 \tag{1}$$

$$I_{f+} = I_3 + I_4 \tag{2}$$

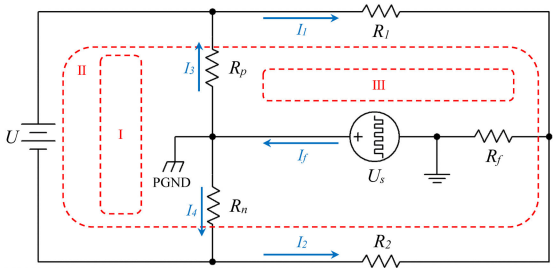

FIGURE 1. Insulation detection circuit model based on the low-frequency signal injection method.

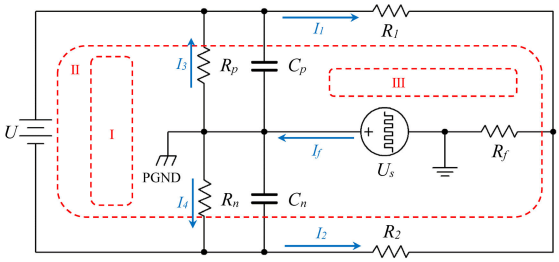

FIGURE 2. Insulation detection circuit model with the Y capacitor.

$$U = R_n I_4 - R_p I_3 \tag{3}$$

$$U = R_1 I_1 - R_2 I_2 \tag{4}$$

$$U_{s+} = R_p I_3 + R_1 I_1 + R_f I_{f+} \tag{5}$$

According to (1)-(5), the voltage U_{f+} across the sampling resistor R_f in the positive half period can be obtained as:

$$U_{f+} = R_f \frac{U(R_p - R_n) + 2U_{s+}(R_p + R_n)}{(R + 2R_f)(R_p + R_n) + 2R_p R_n} \tag{6}$$

Similarly, in the negative half period, the voltage U_{f-} at both ends of the sampling resistor R_f is:

$$U_{f-} = R_f \frac{U(R_p - R_n) + 2U_{s-}(R_p + R_n)}{(R + 2R_f)(R_p + R_n) + 2R_p R_n} \tag{7}$$

When the insulation resistances R_p and R_n remain unchanged in a pulse period, according to (6) and (7), respectively, the insulation resistances R_p and R_n of the two poles of the power battery relative to the vehicle chassis can be obtained as follows:

$$R_p = \frac{(R + 2R_f)(U_{f+}U - U_{f-}U) + 2R_f U(U_{s-} - U_{s+})}{-2U_{f+}U_{s-} + 2U_{f-}U_{s+} + U(U_{f-} - U_{f+})} \tag{8}$$

$$R_n = \frac{(R + 2R_f)(U_{f+}U - U_{f-}U) + 2R_f U(U_{s-} - U_{s+})}{2U_{f+}U_{s-} - 2U_{f-}U_{s+} + U(U_{f-} - U_{f+})} \tag{9}$$

The voltages U_{s+} and U_{s-} generated by the pulse signal generator in the positive and negative cycles are set values. The power battery voltage U can be measured by the high-voltage measuring circuit, and the voltages U_{f+} and U_{f-} on the sampling resistor can be measured by the sampling circuit in the positive and negative cycles. Therefore, as long as the corresponding U_{f+}, U_{f-}, and U are measured in a signal period, the corresponding insulation resistances R_p and R_n in the period can be calculated by (8) and (9), respectively.

B. REFLECTED WAVE VOLTAGE MODEL AFFECTED BY Y CAPACITOR

Considering the influence of the Y capacitance between the positive and negative poles of the power battery and the chassis of the vehicle on the measurement of the insulation resistance, an insulation detection circuit model with the Y capacitance is constructed based on the low-frequency signal injection method, as shown in Fig. 2, and the step response of the circuit model with respect to the pulse injection signal is analyzed.

In Fig. 2, U is the power battery voltage, U_s is the pulse signal generator, R_p and R_n are the power battery positive and negative insulation resistors, respectively, C_p and C_n are positive and negative Y capacitors, respectively, R_1 and R_2 are current limiting resistors, $R_1 = R_2 = R$, and R_f is the sampling resistance. When the pulse generator generates a step voltage with an amplitude of U_s, the currents flowing over R_1, R_2, and R_f are set to I_1, I_2, and I_f, respectively. The sum of the current flowing to R_p and C_p is I_3, the sum of the current flowing to R_n and C_n is I_4, and the initial voltage values of capacitors C_p and C_n are U_{p0} and U_{n0}, respectively. U and R_p, R_n form loop I, U and R_1, R_2 form loop II, and U_s and R_p, R_1, R_f form loop III. According to Kirchhoff's Law, the formula for s-domain is as follows:

$$I_f(s) = I_1(s) + I_2(s) \tag{10}$$

$$I_f(s) = I_3(s) + I_4(s) \tag{11}$$

$$U(s) = \frac{R_n(I_4(s) + C_n U_{n0})}{1 + sC_n R_n} - \frac{R_p(I_3(s) + C_p U_{p0})}{1 + sC_p R_p} \tag{12}$$

$$U(s) = R_1 I_1(s) - R_2 I_2(s) \tag{13}$$

$$U_s(s) = \frac{R_p(I_3(s) + C_p U_{p0})}{1 + sC_p R_p} + R_1 I_1(s) + R_f I_f(s) \tag{14}$$

Sorting out (10)-(14), the reflected wave voltage U_f across the sampling resistor R_f can be obtained, and the inverse Laplace transform can be performed to obtain:

$$U_f(t) = a_1 + a_2 \exp(-t/a_3) \tag{15}$$

Equation (15) is a function of the voltage of the sampling resistance varying with time in a half period, where t is a time variable and the function parameter expression is:

$$a_1 = \frac{R_f(U(R_p - R_n) + 2U_s(R_p + R_n))}{(R_p + R_n)(R + 2R_f) + 2R_p R_n} \tag{16}$$

$$a_3 = \frac{(C_p + C_n)R_p R_n(R + 2R_f)}{(R_p + R_n)(R + 2R_f) + 2R_p R_n} \tag{17}$$

where a_1 is the steady-state component of the response, which is the stationary value of the reflected wave voltage. a_2 is a response gain, which is independent of the calculation of the

resistance and capacitance values and is not considered in this paper. a_3 is the response time constant of the equivalent Y capacitance.

The equivalent Y capacitance value can be obtained by (17), that is, the parallel value of capacitance C_p and C_n:

$$C_p//C_n = a_3 \frac{(R_p + R_n)(R + 2R_f) + 2R_pR_n}{R_pR_n(R + 2R_f)} \tag{18}$$

where $C_p//C_n$ represents the equivalent Y capacitance value.

In summary, the insulation resistances R_p and R_n can be calculated by the identified a_1 value and (8) and (9), and the equivalent Y capacitance value can be calculated by the identified a_3 value and (18).

III. PARAMETER IDENTIFICATION METHOD BASED ON THE VFFRLS ALGORITHM

A. FORGETTING FACTOR RLS ALGORITHM

It can be found from (15) that the reflected wave voltage U_f is a nonlinear model under t. Considering the computational complexity and estimation accuracy, the first-order Taylor series expansion is used to linearize it.

According to (15), the discrete time function of U_f can be obtained, and its expression is as follows:

$$\begin{aligned} U_f(k) &= a_1(k) + a_2(k)\exp(-k\Delta t/a_3(k)) \\ &= F(A(k), k) \end{aligned} \tag{19}$$

where Δt is the sampling interval.

$$A(k) = [a_1(k)\ a_2(k)\ a_3(k)]^\top \tag{20}$$

The linearization method of (19) is as follows. Expand $U_f(k)$ around the estimated value $\hat{A}(k-1)$ at time $k-1$ into a Taylor series, omitting the quadratic and above terms, so that the equation can be reduced to:

$$\begin{aligned} U_f(k) \approx\ & F(\hat{A}(k-1), k) \\ & + (A(k) - \hat{A}(k-1))\frac{\partial F}{\partial A^\top}\Big|_{A(k)=\hat{A}(k-1)} \end{aligned} \tag{21}$$

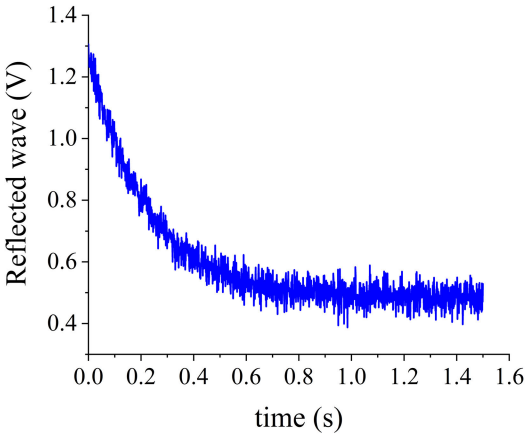

FIGURE 3. Positive half-period reflected wave voltage when $R_p = R_n =$ 2000 kΩ and $C_p = C_n = 0.2$ μF.

where $\hat{A}(k-1)$ represents the parameter estimation value at time $k-1$. The above formula can be written as a regression equation of least squares, and its expression is:

$$U_f(k) = H(k)A(k) + Y(k) + V(k) \tag{22}$$

where

$$H(k) = [1 \quad e^{-\frac{k\Delta t}{\hat{a}_3(k-1)}} \quad \frac{\hat{a}_2(k-1)k\Delta t e^{-\frac{k\Delta t}{\hat{a}_3(k-1)}}}{\hat{a}_3^2(k-1)}] \tag{23}$$

$$Y(k) = -\frac{\hat{a}_3(k-1)\hat{a}_2(k-1)k\Delta t e^{-\frac{k\Delta t}{\hat{a}_3(k-1)}}}{\hat{a}_3^2(k-1)} \tag{24}$$

Equation (22) can be regarded as a model with constant error term $Y(k)$ in the observation equation. $H(k)$ is the observation matrix, $V(k)$ is one-dimensional random observation noise, which is a zero mean and independent white Gaussian noise sequence.

The forgetting factor RLS algorithm is used to identify the model parameters. The implementation process of the algorithm is shown in Table 1.

TABLE 1. The implementation process of the forgetting factor RLS algorithm.

1. Initialization

Parameter initial value: $\hat{A}(0)$, *Initial value of error covariance:* $P(0)$, *Forgetting factor:* λ

2. Calculate the observation matrix

$$H(k) = [1 \quad \exp(-k\Delta t / \hat{a}_3(k-1)) \quad \hat{a}_2(k-1)k\Delta t \exp(-k\Delta t / \hat{a}_3(k-1)) / \hat{a}_3^2(k-1)] \tag{25}$$

3. Calculate the gain

$$K(k) = P(k-1)H^\top(k)[\lambda + H(k)P(k-1)H^\top(k)]^{-1} \tag{26}$$

4. Calculate the estimated value

$$\hat{A}(k) = \hat{A}(k-1) + K(k)[U_f(k) - F(\hat{A}(k-1), k)] \tag{27}$$

5. Update error covariance matrix

$$P(k) = [1 - K(k)H(k)]P(k-1) / \lambda \tag{28}$$

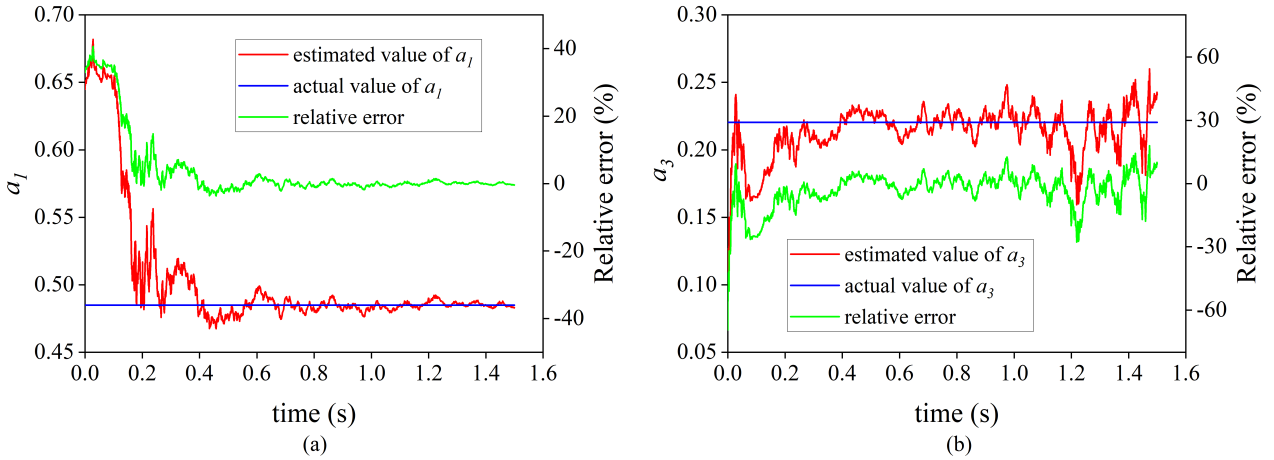

FIGURE 4. The identification process when the forgetting factor is 0.99: (a) the identification process of a_1 and (b) the identification process of a_3.

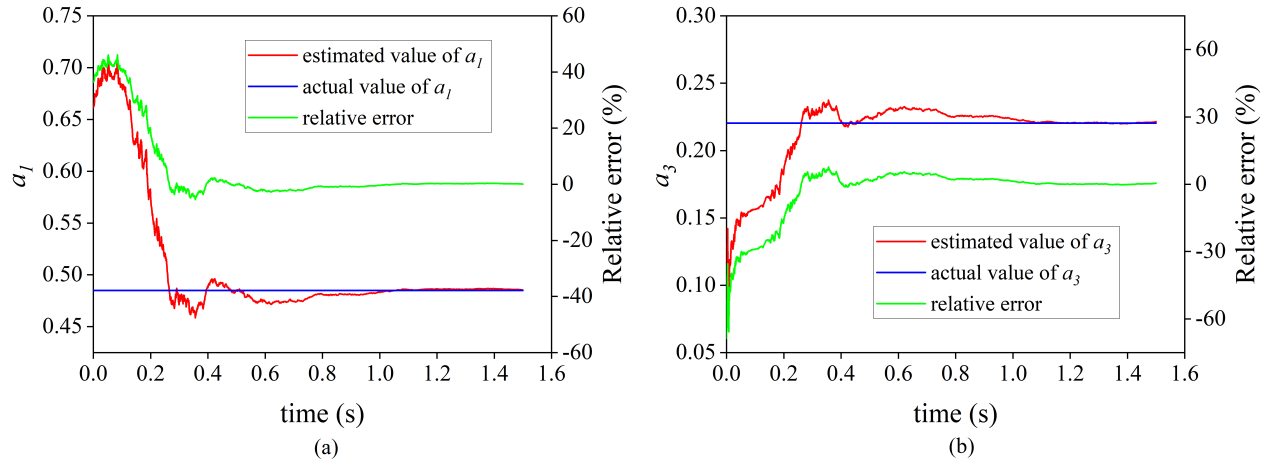

FIGURE 5. The identification process when the forgetting factor is 1: (a) the identification process of a_1 and (b) the identification process of a_3.

B. VARIABLE FORGETTING FACTOR

In the RLS algorithm, the forgetting factor λ is mainly used to increase the weight of the current data. The idea is to add the forgetting factor to the old data and attenuate the influence of the old data on identification in the form of exponential weighting. The cost function of the forgetting factor RLS algorithm is

$$J(n) = \sum \lambda^{n-i} e^2(i) \tag{29}$$

where $i = 1, 2 \ldots, n, 0 < \lambda \leq 1, e(i)$ represents the difference between the observed value and the estimated value at time i. By analyzing the recursive formula in Table 1, it is found that the larger the λ value is, the smaller the gain $K(k)$, which reduces the correction effect of the observation data on the parameter estimation and thus leads to the slower convergence speed of the algorithm. However, it is not sensitive to noise. The estimation error of the parameter is also smaller. In the same way, if the value of λ is smaller, then the convergence speed is faster, but it is more sensitive to noise, and the estimation error of the parameter at convergence is also larger [33], [34].

To obtain the influence of different λ values on the convergence speed and parameter estimation, set the insulation resistance $R_p = R_n = 2000$ kΩ, the Y capacitance $C_p = C_n = 0.2$ μF, the power battery voltage $U = 300$ V, and the pulse injection voltage amplitude $U_s = 40$ V. The positive half-period reflected wave voltage data shown in Fig. 3 are obtained through simulation, and the data noise variance is 0.001. Due to the charging process of the Y capacitor, the reflected wave voltage decreases exponentially, and as time increases, the voltage gradually stabilizes, which conforms to the description of (15). By identifying with the forgetting factor RLS algorithm, the identifying processes with the forgetting factor equal to 0.99 and 1 are obtained, as shown in Figs. 4 and 5, respectively. Figs. 4(a) and 5(a) show the identification process of parameter a_1, and Figs. 4(b) and 5(b) show the identification process of parameter a_3. Through comparison, it can be found that when $\lambda = 0.99$, the identification process converges

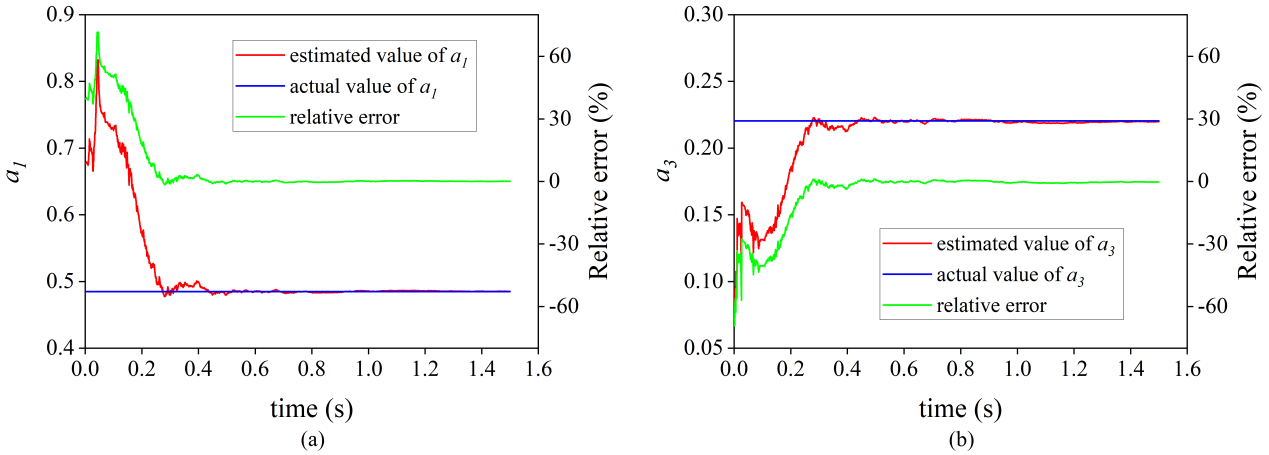

FIGURE 6. The identification process when the variable forgetting factor: (a) the identification process of a_1 and (b) the identification process of a_3.

faster, starting to converge in approximately 0.6 s, but the convergence accuracy is relatively low, and the parameters a_1 and a_3 fluctuate greatly. When $\lambda = 1$, the convergence accuracy is relatively high, and the fluctuations of parameters a_1 and a_3 are also relatively small, but the convergence speed is slower and starts to converge in approximately 1.0 s. In addition, in Fig. 4(b), since $\lambda < 1$ and the reflected wave voltage gradually stabilized after 1.0 s, the identification error of a_3 begins to increase after 1.0 s. Therefore, when designing the forgetting factor RLS algorithm, the selection of the λ value is very important, and it should be considered as a compromise between the convergence speed and stability of the algorithm.

In view of the characteristics of the system reflected wave voltage signal, it is hoped that when the injected square wave signal changes between positive and negative values, λ takes a smaller value so that the system can quickly track the signal trend and improve the dynamic response speed. When the algorithm starts to converge, a larger λ value is used to obtain a smaller steady-state error of the system and improve the accuracy of convergence. Since the fixed forgetting factor cannot take into account the requirements of accuracy and convergence speed [35], this paper proposes a variable forgetting factor method to achieve both accuracy and convergence speed. The variable forgetting factor is defined as follows:

$$\lambda(k) = \lambda_1 - (\lambda_1 - \lambda_0)\exp(-\beta k \Delta t) \tag{30}$$

where λ_0, λ_1, and β are the parameters for calculating the forgetting factor. The parameter values used in this article are $\lambda_0 = 0.96$, $\lambda_1 = 1$, and $\beta = 40$. It can be determined from (30) that after the injected signal changes between positive and negative values, λ will gradually increase from a smaller value of 0.96 to 1 until the algorithm reaches the set convergence accuracy. By simulating the VFFRLS algorithm, the results shown in Fig. 6 are obtained. It can be found from the figure that the algorithm starts to converge in 0.4 s, the convergence accuracy is relatively high, and the fluctuations of parameters a_1 and a_3 are relatively small. The results show that the variable forgetting factor RLS algorithm is better than the fixed forgetting factor in terms of the convergence speed and convergence accuracy.

C. ALGORITHM IMPLEMENTATION

In the process of using the VFFRLS algorithm to identify model parameters, the stopping condition of the algorithm is one of the key factors affecting the effectiveness of the algorithm. If it stops prematurely, then the algorithm does not converge at this time, and the error of the identification result is large. If the shutdown occurs too late, then the measurement period will increase, which reduces the response speed of the measurement system, wastes substantial computing resources, and may also increase the number of errors. As shown in Fig. 4(b), in the process of identifying a_3 when $\lambda = 0.99$, the reflected wave voltage tends to be stable in the later stage, causing the error to increase again. Therefore, it is necessary to determine whether the algorithm converges on the basis of weighing the identification accuracy and the measurement period to establish an appropriate shutdown criterion. The specific process of judging whether the algorithm has converged is shown in Fig. 7. When the standard deviation of a_1 and a_3 in the sliding window is less than ε at the same time, the algorithm is considered to have converged and the iteration is exited. Using the form of the standard deviation within the sliding window can effectively determine whether the algorithm has converged, control the stopping of the algorithm, and avoid misjudgment of the convergence.

Fig. 8 is the implementation flow chart of the insulation resistance measurement method proposed in this paper. First, the initial value and parameters of the algorithm are set. Then, the VFFRLS algorithm is used to identify the model parameters. When the convergence accuracy is reached, the average values of a_1 and a_3 in the sliding window are used as the result of parameter identification. Finally, the insulation resistance value is calculated by (8) and (9), and the equivalent Y capacitance value is calculated by (18).

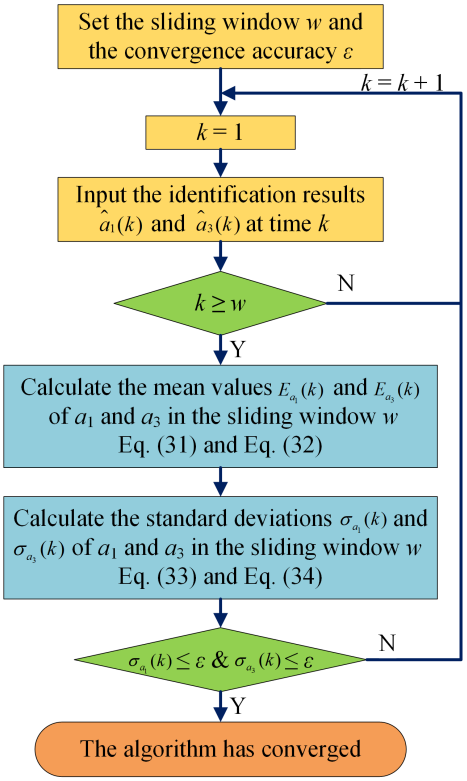

FIGURE 7. The flow chart of judging whether the algorithm has converged.

The calculation formulas for the mean values $E_{a_1}(k)$ and $E_{a_3}(k)$ and the standard deviations $\sigma_{a_1}(k)$ and $\sigma_{a_3}(k)$ are as follows:

$$E_{a_1}(k) = \frac{1}{w} \sum_{i=k-w+1}^{k} \hat{a_1}(i) \tag{31}$$

$$E_{a_3}(k) = \frac{1}{w} \sum_{i=k-w+1}^{k} \hat{a_3}(i) \tag{32}$$

$$\sigma_{a_1}(k) = \sqrt{\frac{1}{w} \sum_{i=k-w+1}^{k} (\hat{a_1}(i) - E_{a_1}(k))^2} \tag{33}$$

$$\sigma_{a_3}(k) = \sqrt{\frac{1}{w} \sum_{i=k-w+1}^{k} (\hat{a_3}(i) - E_{a_3}(k))^2} \tag{34}$$

IV. SIMULATION AND EXPERIMENTAL CONFIGURATION

To verify the electric vehicle insulation detection method based on the VFFRLS algorithm proposed in this paper, simulation experiments and bench experiments were carried out under different insulation resistances and Y capacitances. The parameters of the insulation detector system in the process of the simulation experiment and bench experiment are shown in Table 2. In the actual use of electric vehicles, a long transition time is required for the insulation resistance and Y capacitance values to change. However, considering that the model parameters change slowly, it is difficult to verify the rapidity and accuracy of the identification algorithm convergence. Therefore, in the experiment, the insulation resistance value and the Y capacitance value were changed artificially to cause a sudden change.

TABLE 2. The parameters of the insulation detector system.

Items		Values
The current limiting resistors R_1, R_2 ($R_1 = R_2$)		2400 kΩ
Sampling resistor R_f		27 kΩ
Injection voltage amplitude U_s		40 V
Parameters for judging convergence	w	8
	ε	0.0001
Parameters of forgetting factor	λ_0	0.96
	λ_1	1
	β	40

A. SIMULATION CONFIGURATION

The simulation model of the system is established using MATLAB software, as shown in Fig. 9. Fig. 9(a) depicts a circuit simulation model that generates the required data by simulating the high-voltage circuit and insulation detection circuit of electric vehicles. R_p and R_n are the insulation resistances, C_p and C_n are the Y capacitors, R_1 and R_2 are the current limiting resistors, R_f is a sampling resistor, U_s is an injection voltage signal, and the power battery voltage is 300 V. Fig. 9(b) shows the VFFRLS model. The input of the model is the data obtained by the simulation in Fig. 9(a), and the output is the identified a_1 and a_3. The model mainly consists of a time module, an observation matrix module, a forgetting factor module, a gain module, an estimated value update module, an error variance update module, and a judgment convergence module. In the simulation experiment, the fixed-step calculation mode is adopted, and the simulation step is set to 0.001 s according to a sampling frequency of 1 kHz.

B. EXPERIMENTAL CONFIGURATION

The structure of the test bench is shown in Fig. 10. The test bench mainly consists of a high-voltage DC power supply, an insulation detector, a low-voltage DC power supply, two DC resistance boxes, two decimal adjustable capacitor boxes, a CAN monitor, a downloader and a personal computer (PC). The high-voltage DC power system is used to simulate the power battery voltage and is set to 300 V. The low-voltage DC power system supplies power to the insulation detector, and the power supply voltage of the insulation detector is 12 V. The two DC resistance boxes simulate the insulation resistance of the positive and negative electrodes. The two capacitor boxes simulate positive and negative Y capacitors. The PC downloads the software project file to the micro-control unit (MCU) of the insulation detector through the downloader and collects experimental data such as the power battery voltage, injection voltage signal, reflected wave voltage signal,

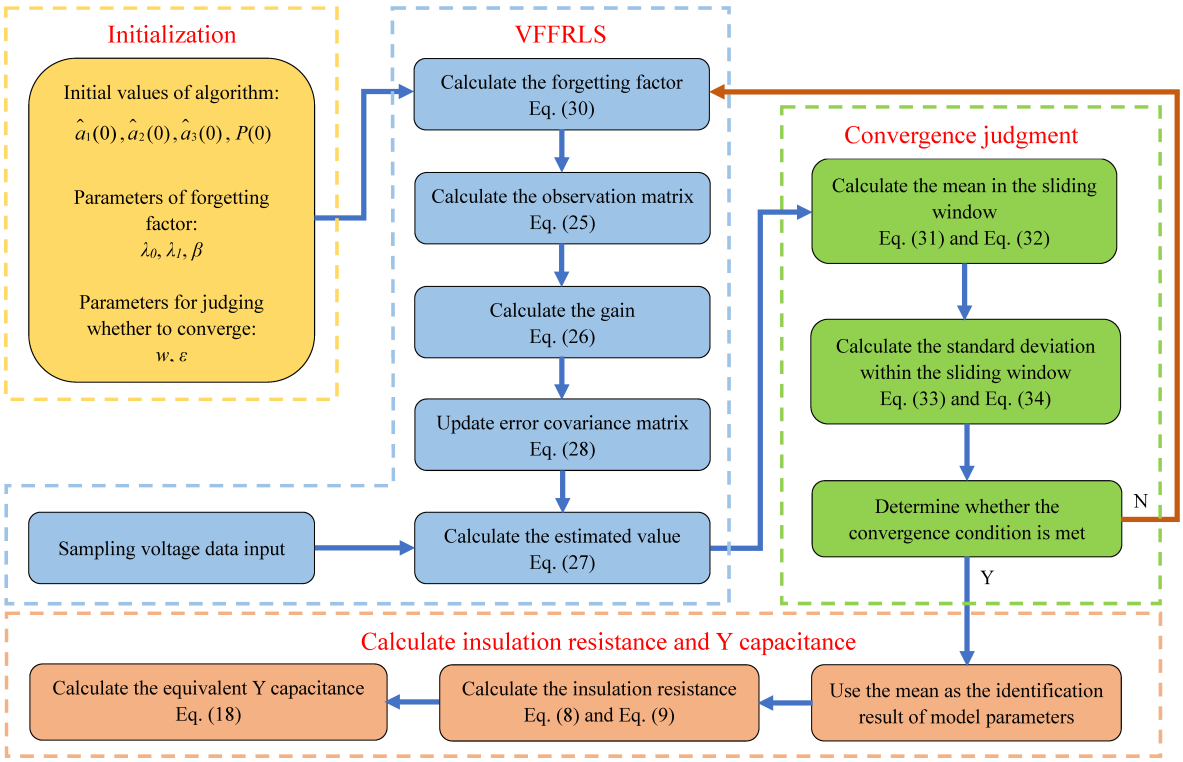

FIGURE 8. Flowchart of the insulation resistance estimation based on VFFRLS.

and insulation resistance measurement value through a CAN monitor.

V. RESULTS AND DISCUSSION

A test bench for the simulation with the configuration shown in Fig. 9 was built using MATLAB software. Three tests were executed to test the performance of the VFFRLS algorithm using the test bench for the simulation. The system cost should be lower for the electrical vehicle, so the hardware of insulation detection was designed for the lower cost. Freescale's KEA128 was used as an embedded MCU to test the performance of the proposed method with respect to the system cost. Hardware was designed with the selected MCU, a test bench was built, and three tests were executed to test the performance of the proposed method with the configuration of Fig. 10.

A. EXPERIMENT 1: SIMULATIONS WITHOUT/WITH MEASURING NOISE

The reflected wave voltage data, as shown in Fig. 11, are obtained through Simulink simulation. The injection signal cycle is 3 s, the simulation time is 12 s, and a total of 4 cycles are simulated. The blue curve represents the reflected wave voltage data without noise. To simulate the actual reflected wave voltage value, Gaussian white noise with a variance of 0.01 is superimposed on the signal sampling end to obtain the red curve in Fig. 11. The model parameters exhibit sudden change at the end of each cycle, and the insulation resistance and Y capacitance values of the four cycles are shown in Table 3.

TABLE 3. Insulation resistance and Y capacitance value of Four cycles.

	R_p (kΩ)	R_n (kΩ)	C_p (μF)	C_n (μF)
First cycle	2000	2000	0.1	0.4
Second cycle	1800	300	0.3	0.3
Third cycle	200	1000	0.5	0.2
Fourth cycle	100	100	0.3	0.5

Using the reflected wave voltage data without noise for the simulation, the measurement results shown in Table 4 are obtained, where $\overline{R_p}$ and $\overline{R_n}$ are the measurement results of the positive and negative insulation resistances, respectively, $\overline{C_p//C_n}$ is the measurement result of the equivalent Y capacitance, and δ is the relative error. It can be found from the table that the relative error of measurement is within 1% and the measurement time T is within 0.3 s without noise. The insulation resistance and Y capacitance can be accurately and quickly measured.

The simulation is carried out using reflected wave voltage data with a noise variance of 0.01. Each set of data is simulated ten times, the average values are taken as the measurement results of the insulation resistance and the Y capacitance value, and the measurement results shown in Table 5 are obtained. It can be determined from the table that in the

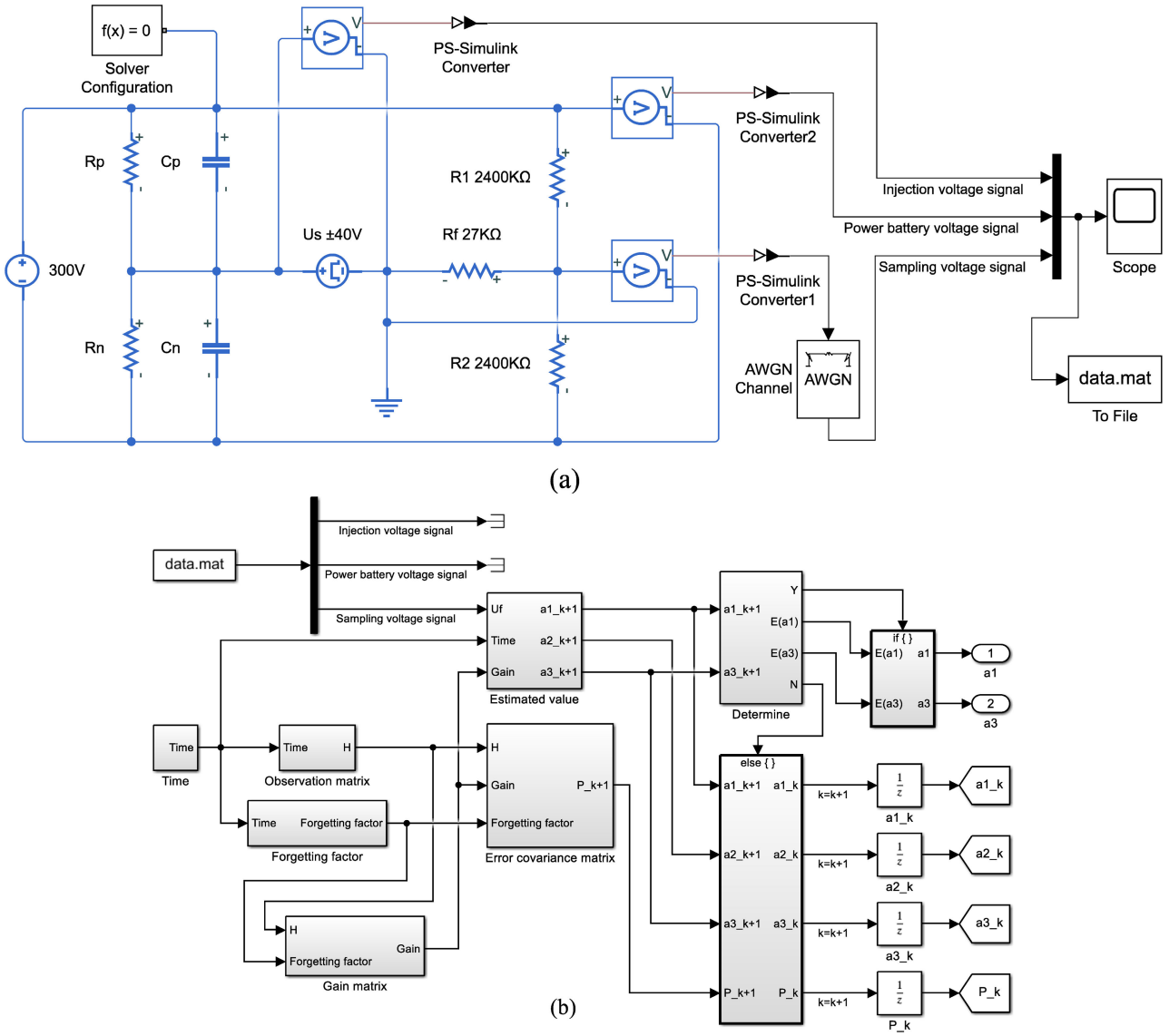

FIGURE 9. Simulation model of the insulation detection system: (a) the insulation detection circuit model and (b) the VFFRLS model.

TABLE 4. Measurement results without noise.

Consequence	$\overline{R_p}$ (kΩ)	δ (%)	RMSE (kΩ)	$\overline{R_n}$ (kΩ)	δ (%)	RMSE (kΩ)	$\overline{C_p//C_n}$ (μF)	δ (%)	RMSE (μF)	Measurement period T (s)
First cycle	2008.3	0.415	8.3	2010.4	0.52	10.4	0.497	-0.6	0.003	0.234
Second cycle	1792.1	-0.439	7.9	298.3	-0.567	1.663	0.604	0.667	0.004	0.238
Third cycle	200.6	0.3	0.6	1005.4	0.54	5.4	0.704	0.571	0.004	0.210
Fourth cycle	99.7	-0.3	0.3	99.6	-0.4	0.4	0.795	-0.625	0.005	0.208

presence of noise interference, the relative measurement error of insulation resistance is within 1.8%, and the relative measurement error of the Y capacitor is within 1.9%. VFFRLS effectively reduces noise interference.

Through simulation, compare EKF, unscented Kalman filter (UKF) and the algorithm proposed in this paper. The three algorithms adopt the same initial value and convergence condition. When using noisy data for simulation, it was found that EKF and UKF diverged. Therefore, the data without noise in the second cycle is selected for simulation, and the results are shown in Table 6. The results show that in the absence of noise, the convergence speed of EKF and

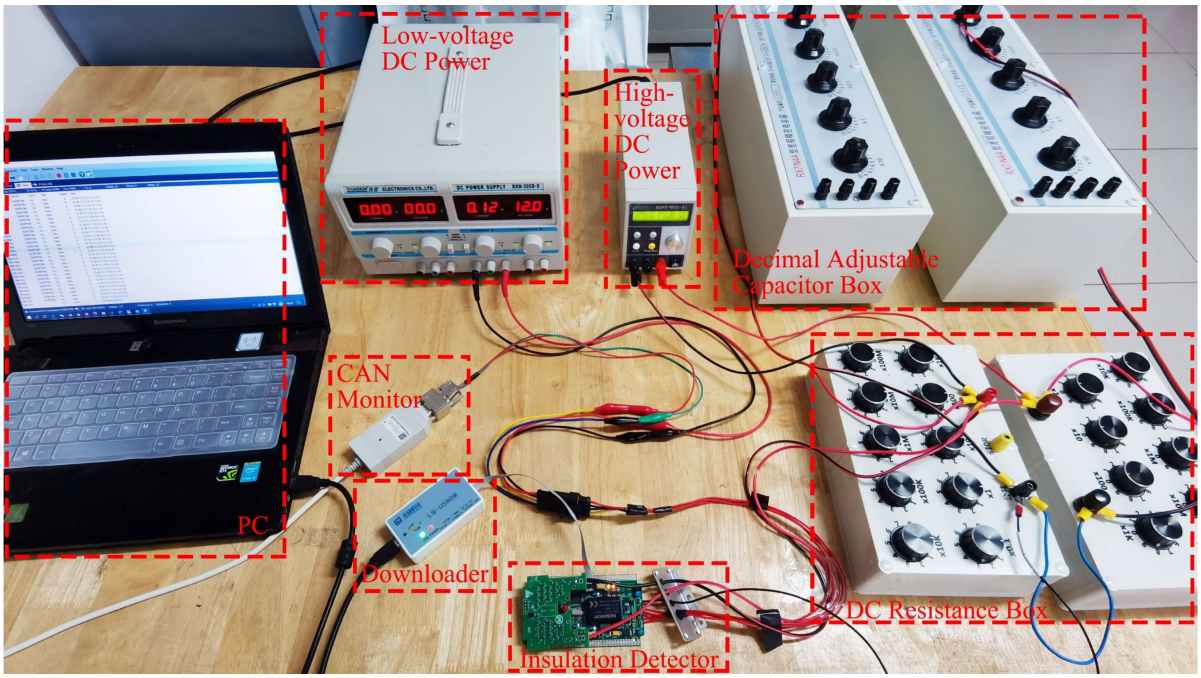

FIGURE 10. Insulation resistance test bench.

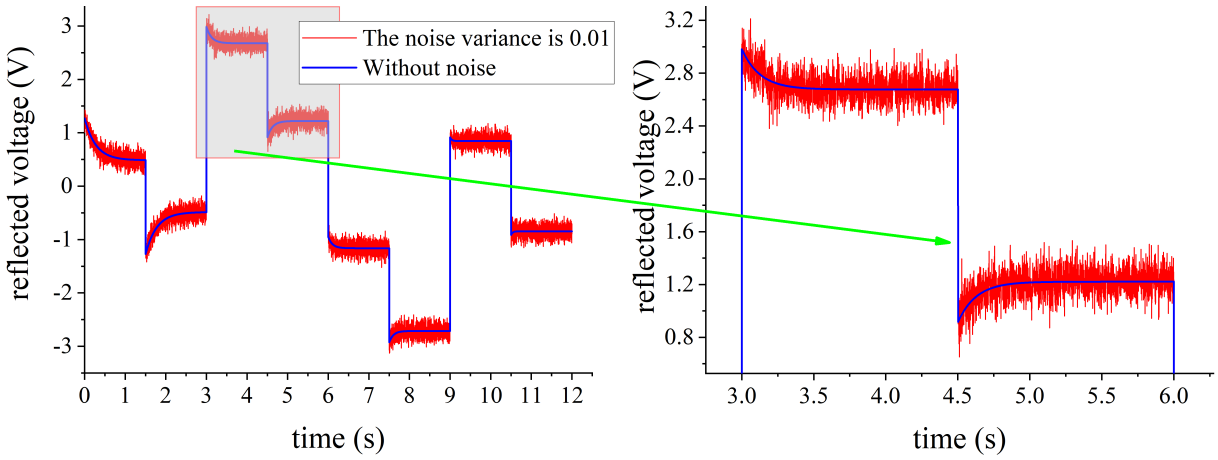

FIGURE 11. Reflected wave voltage data.

TABLE 5. Measurement results with a noise variance of 0.01.

Consequence	$\overline{R_p}$ (kΩ)	δ (%)	RMSE (kΩ)	$\overline{R_n}$ (kΩ)	δ (%)	RMSE (kΩ)	$\overline{C_p//C_n}$ (μF)	δ (%)	RMSE (μF)	Measurement period T (s)
First cycle	2034.7	1.735	50.87	2033.0	1.65	49.76	0.503	0.6	0.009	1.165
Second cycle	1773.3	-1.483	43.96	297.4	-0.867	4.355	0.61	1.667	0.026	0.910
Third cycle	201.8	0.9	4.203	1011.5	1.15	26.2	0.71	1.43	0.028	0.750
Fourth cycle	101.6	1.6	2.811	101.6	1.6	2.799	0.815	1.88	0.024	0.498

UKF is faster than the VFFRLS algorithm, and the measurement accuracy of the VFFRLS is higher than EKF, but slightly lower than UKF. The simulation results show that although UKF is better than VFFRLS, when there is noise, UKF and EKF will diverge, and VFFRLS can run smoothly.

TABLE 6. Measurement results of different algorithms.

Consequence	$\overline{R_p}$ (kΩ)	δ (%)	RMSE (kΩ)	$\overline{R_n}$ (kΩ)	δ (%)	RMSE (kΩ)	$\overline{C_p//C_n}$ (μF)	δ (%)	RMSE (μF)	Measurement period T (s)
VFFRLS	1792.1	-0.439	7.9	298.3	-0.567	1.663	0.604	0.667	0.004	0.238
EKF	1788.82	-0.621	9.897	297.51	-0.83	2.231	0.6053	0.883	0.006	0.194
UKF	1794.64	-0.298	5.623	298.73	-0.423	1.121	0.6026	0.433	0.003	0.134

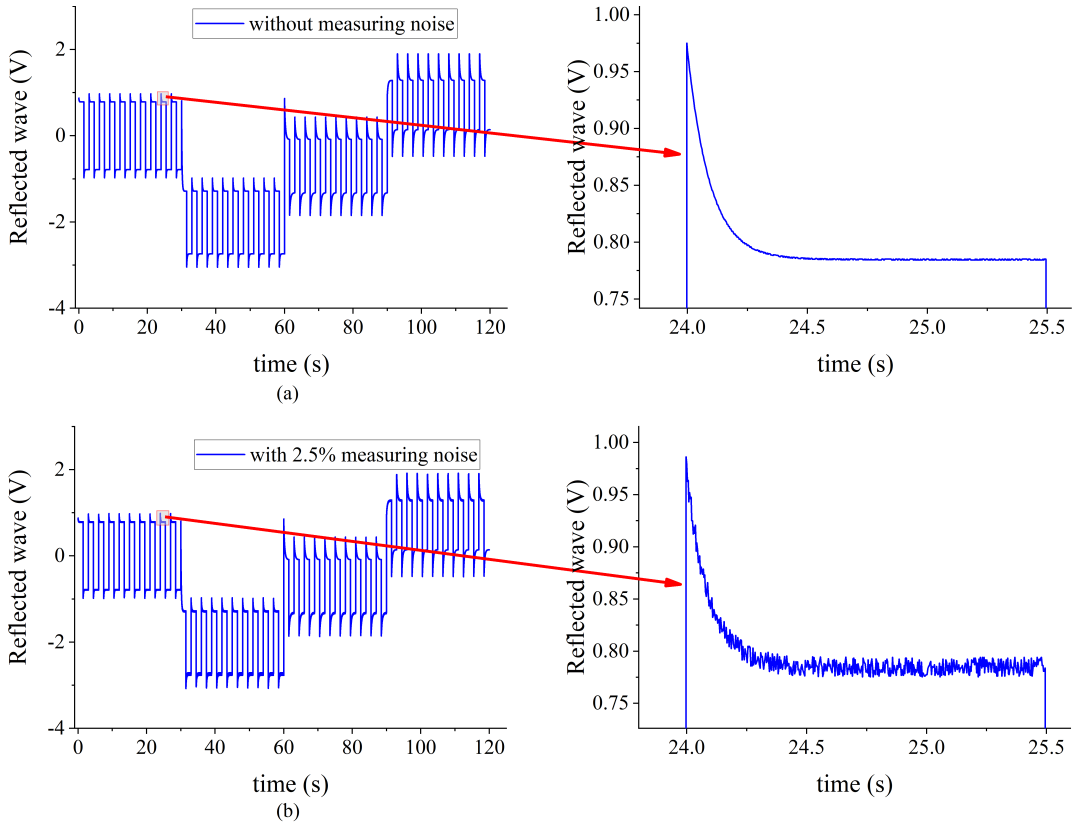

FIGURE 12. Reflected wave voltage data without measuring noise and with measuring noise of reflected wave: (a) without measuring noise and (b) with 2.5% measuring noise.

B. EXPERIMENT 2: COMPUTING COMPLEXITY TEST

To verify the computing complexity of the proposed algorithm, a contrast test with an EKF, an UKF and the proposed algorithm is executed. The bus frequency is set to 48 MHz, the programs are executed once every 3 ms, the period of the reflected wave is 3 s, and the results are shown in Table 7. It is shown that the computing complexity of the proposed algorithm is the lowest among the three algorithms. The load rate of the KEA128 embedded MCU is lower than 70% when running the program of the proposed algorithm. This result shows that the VFFRLS algorithm for insulation detection can run smoothly on the KEA128 embedded MCU.

TABLE 7. Computing complexity of different algorithms.

Estimation methods	EKF	UKF	VFFRLS
Load rate (%)	92.3	100	68.8

C. EXPERIMENT 3: TESTS WITHOUT AND WITH MEASURING NOISE

To verify the performance of the VFFRLS algorithm in an actual demo with the test bench shown in Fig. 10, the test requires a total of 300 s and is divided into four time periods. The parameter settings of the insulation resistance and Y capacitor in different time periods are shown in Table 8. The period of the wave is 3 s, so the half period of the reflected wave is 1.5 s.

Electric vehicles have many components with high electromagnetic interference (including a relay, solenoid valve, motor control, motor, etc.) and the operating environment and working conditions are complex. The signal sampling circuit is easily interfered with, and the insulation detection

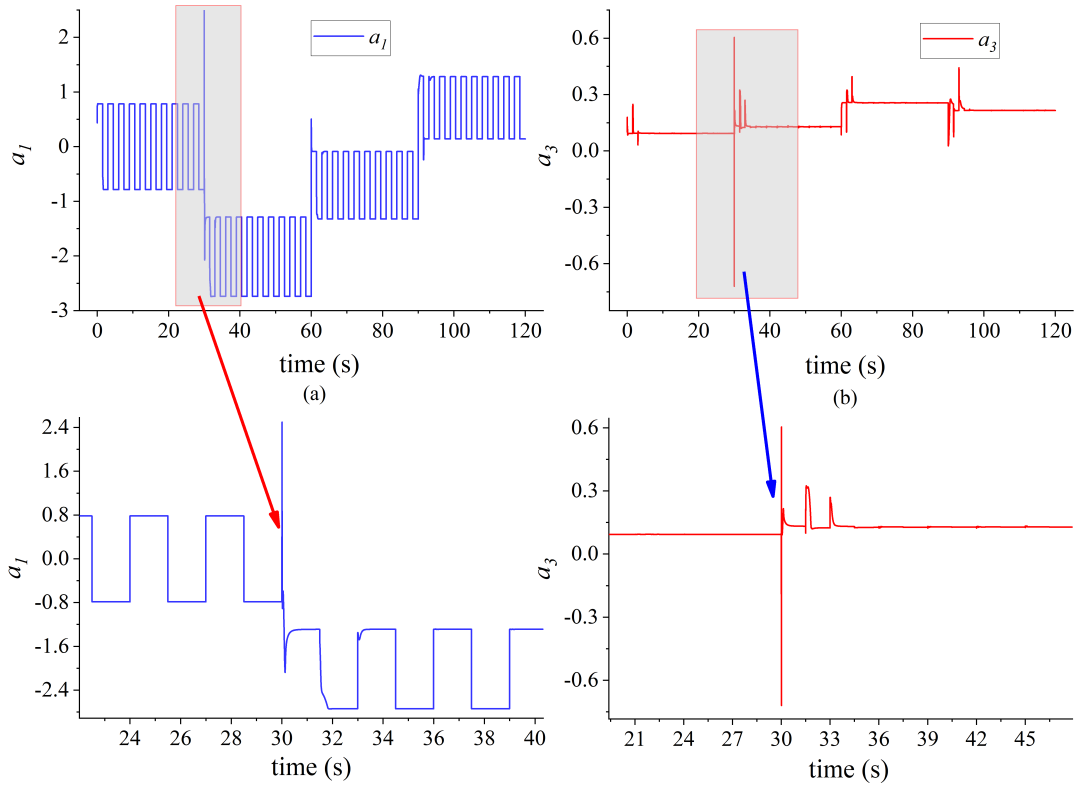

FIGURE 13. Results of a_1 and a_3 without measuring the noise of the reflected wave: (a) estimated a_1 and (b) estimated a_3.

TABLE 8. Working conditions of the tests.

Test time	R_p (kΩ)	R_n (kΩ)	C_p (μF)	C_n (μF)
1-30 s	300	300	0.3	0.4
31-60 s	300	2000	0.3	0.3
61-90 s	800	1500	0.5	0.2
90-120 s	2000	1000	0.2	0.3

algorithm must be useful, with strong anti-interference ability and good robustness. To test the anti-interference performance and robustness of the proposed algorithm, 2.5% sampling signal noise was applied to the reflected wave sampling circuit, and the noise was described as follows:

$$Q = b^* M/3 \tag{35}$$

where Q is the root mean square noise value, b represents the scaling factor, and M is the maximum voltage value of the reflected wave. The measurement noise is loaded with 2.5% of the actual signal. The measured signal of the reflected wave is shown in Fig. 12 without/with measuring noise. Fig. 13 shows the results of the estimated parameters of a_1 and a_3 achieved by the VFFRLS algorithm without measuring noise, and the results of the two parameters are shown in Fig. 14 with measuring noise. Figs. 15-17 are the results of R_p, R_n, and $C_p//C_n$ without and with measuring noise, and Fig. 18 displays the error distribution of the estimation results of R_p, R_n, and $C_p//C_n$.

When the changes in the capacitance or resistance before and after the switching point are small, the fluctuation of the estimated results of a_1 and a_3 is minimal; in contrast, the fluctuation of the estimated results of a_1 and a_3 is large. The results of a_1 can converge to the correct value in one reflected wave period, while a_3 can converge to the correct value in two reflected wave periods. According to the method described in this paper, the values of R_p, R_n, and $C_p//C_n$ are further obtained from the estimated values of a_1 and a_3. At the same time, the calculation of R_p, R_n, and $C_p//C_n$ values requires a complete reflected wave period, so the calculated fluctuation period of R_p, R_n, and $C_p//C_n$ values will be further extended, and the maximum fluctuation time is approximately 8 s in experiment 3. According to the error distribution diagram, with or without the reflected wave measurement error, except for the error during initialization and near the switching point, the relative error of the R_p, R_n, and $C_p//C_n$ parameters in the whole process is less than 2%, and the RMSE is less than 0.012. In practical engineering, limit filtering can be carried out at the switching point to further smooth the fluctuation error caused by large parameter changes during the switching to further improve the estimation accuracy of the whole process. Considering that drastic changes in the capacitance and resistance at 0.003 s are rare under actual work conditions, the maximum fluctuation of the estimated value is approx-

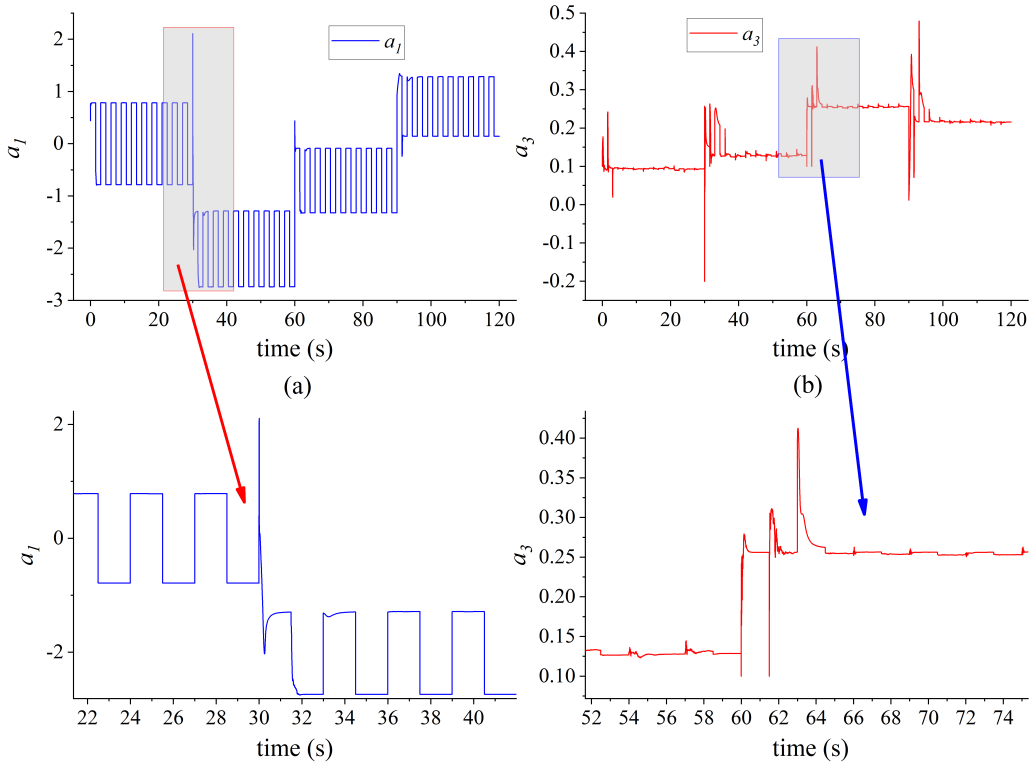

FIGURE 14. Results of a_1 and a_3 with 2.5% measuring noise of reflected wave: (a) estimated a_1 and (b) estimated a_3.

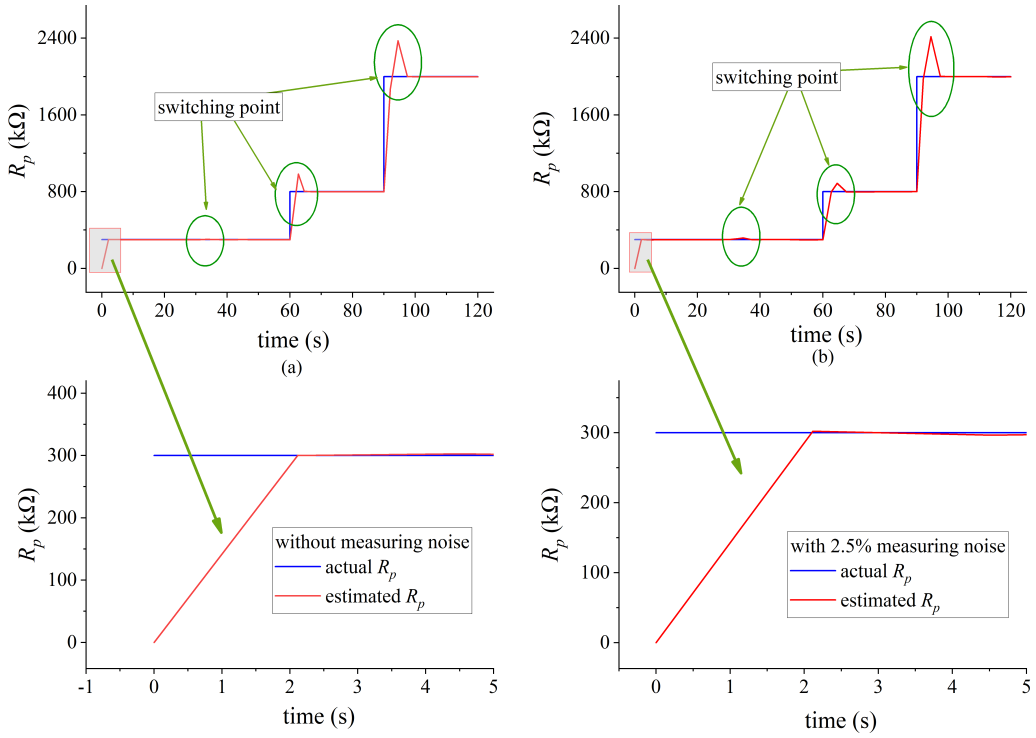

FIGURE 15. Results of R_p without and with 2.5% measuring noise of reflected wave: (a) R_p without measuring noise and (b) R_p with 2.5% measuring noise.

imately 3 s (that is, convergence can be completed in one reflected wave cycle) when the change in working conditions is small.

Therefore, in the cases of different Y capacitors and insulation resistors, the detection accuracy of the insulation resistance is still very high (the RMSE is within 0.012) after

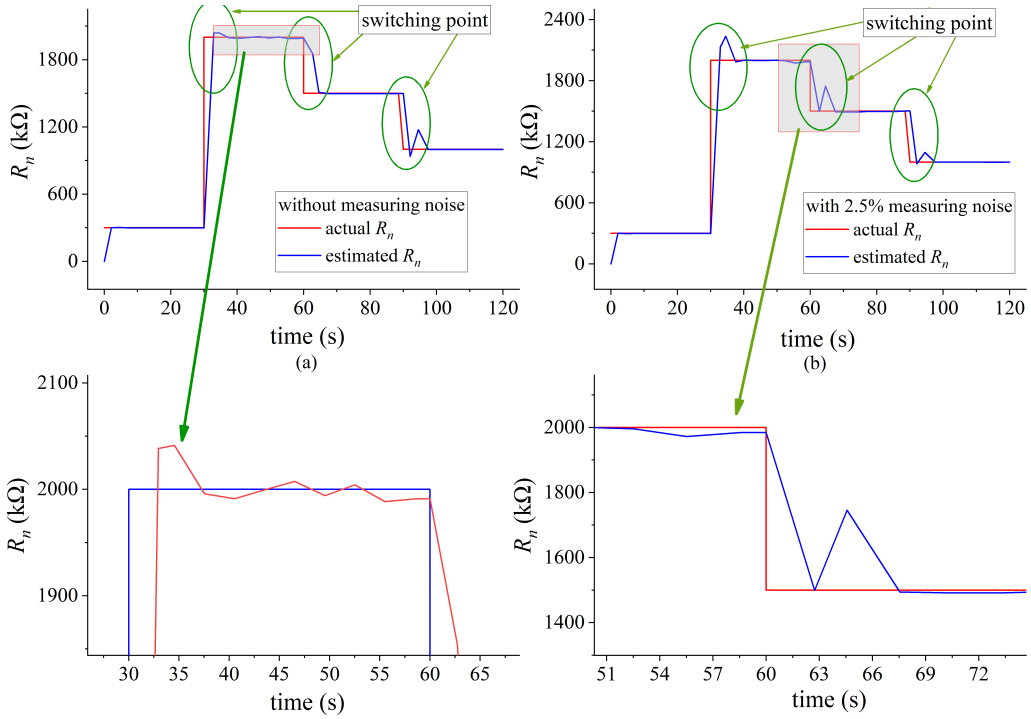

FIGURE 16. Results of R_n without and with 2.5% measuring noise of reflected wave: (a) R_n without measuring noise and (b) R_n with 2.5% measuring noise.

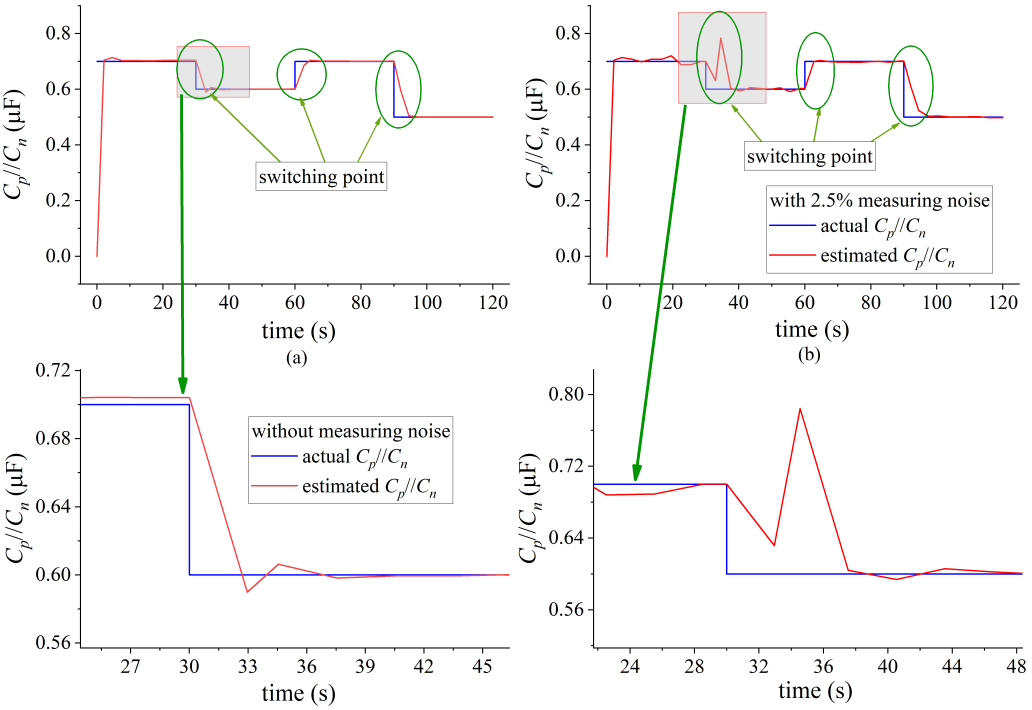

FIGURE 17. Results of $C_p//C_n$ without and with 2.5% measuring noise of reflected wave: (a) $C_p//C_n$ without measuring noise and (b) $C_p//C_n$ with 2.5% measuring noise.

loading the measurement noise with 2.5%, the response speed is very short (the average response time is within 3 s), and the convergence property of the continuous algorithm is still maintained after running continuously. The results show that the proposed method exhibits high anti-interference ability and robustness.

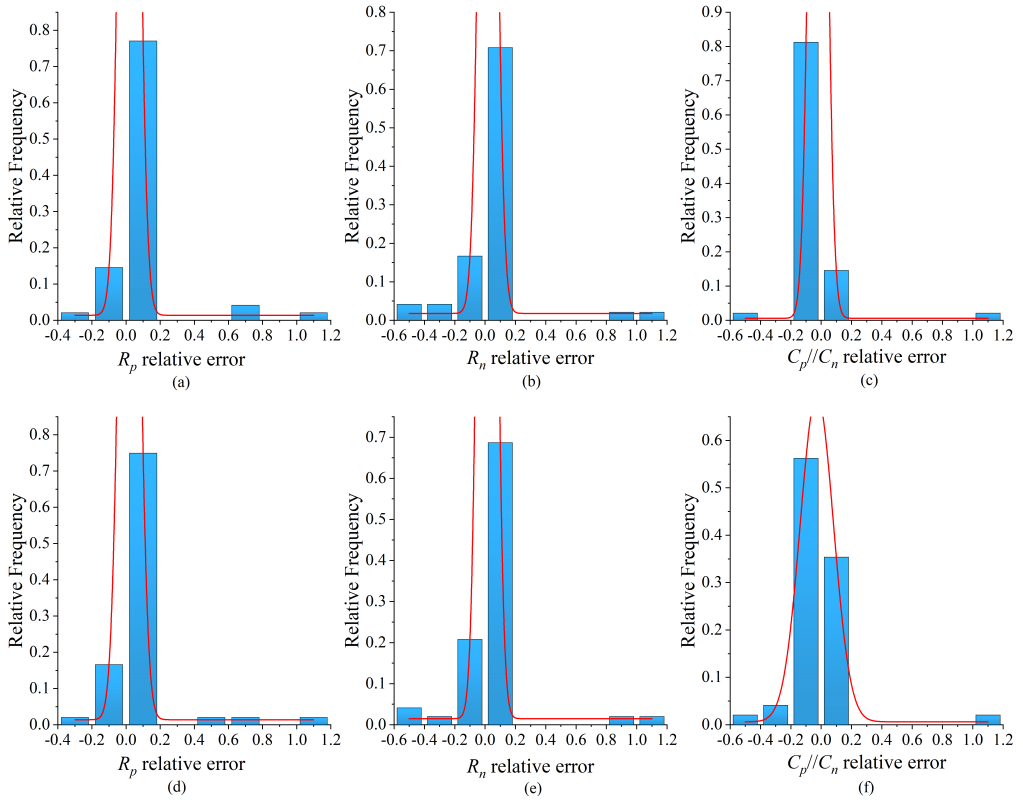

FIGURE 18. Distribution of the relative error of the estimation results: (a) R_P relative error without measuring noise; (b) R_n relative error without measuring noise; (c) $C_P//C_n$ relative error without measuring noise; (d) R_P relative error with measuring noise; (e) R_n relative error with measuring noise; and (f) $C_P//C_n$ relative error with measuring noise.

VI. CONCLUSION

Based on the circuit model of low-frequency signal injection to measure the insulation resistance, the principle of insulation detection is described in detail, and the calculation formula of insulation resistance is derived. Considering the influence of the Y capacitance of the system, a nonlinear reflected wave voltage model is established according to the step response of the injected signal. After linearizing it through a first-order Taylor expansion, the model parameters are identified by the variable forgetting factor recursive least squares algorithm, and the insulation resistance value and Y capacitance value are calculated according to the model parameters. The experimental test results show that the proposed method can quickly track the changes in the insulation resistance and Y capacitance under the condition of noise interference. The root mean square error is within 0.012, and the average response time is within 3 s. Simulation experiments and bench tests prove that this method exhibits the advantages of a fast response speed, high robustness, high estimation accuracy and strong anti-interference ability. At present, this method has been tested on a bench in the laboratory. In future work, the proposed method shall be applied to actual electric vehicles to further verify its performance in realistic environments.

ACKNOWLEDGMENT

The authors would also like to thank Hainan Normal University for the support.

REFERENCES

[1] U. Chong, S. H. L. Yim, S. R. H. Barrett, and A. M. Boies, "Air quality and climate impacts of alternative bus technologies in Greater London," *Environ. Sci. Technol.*, vol. 48, no. 8, pp. 4613–4622, Apr. 2014, doi: 10.1021/es4055274.

[2] J. Remmlinger, M. Buchholz, M. Meiler, P. Bernreuter, and K. Dietmayer, "State-of-health monitoring of lithium-ion batteries in electric vehicles by on-board internal resistance estimation," *J. Power Sources*, vol. 196, no. 12, pp. 5357–5363, Jun. 2011, doi: 10.1016/j.jpowsour.2010.08.035.

[3] S. J. Gerssen-Gondelach and A. P. C. Faaij, "Performance of batteries for electric vehicles on short and longer term," *J. Power Sources*, vol. 212, pp. 111–129, Aug. 2012, doi: 10.1016/j.jpowsour.2012.03.085.

[4] L. Lu, X. Han, J. Li, J. Hua, and M. Ouyang, "A review on the key issues for lithium-ion battery management in electric vehicles," *J. Power Sources*, vol. 226, pp. 272–288, Mar. 2013, doi: 10.1016/j.jpowsour.2012.10.060.

[5] R. Xiong, F. Sun, X. Gong, and H. He, "Adaptive state of charge estimator for lithium-ion cells series battery pack in electric vehicles," *J. Power Sources*, vol. 242, pp. 699–713, Nov. 2013, doi: 10.1016/j.jpowsour.2013.05.071.

[6] R. Adany, D. Aurbach, and S. Kraus, "Switching algorithms for extending battery life in electric vehicles," *J. Power Sources*, vol. 231, pp. 50–59, Jun. 2013, doi: 10.1016/j.jpowsour.2012.12.075.

[7] X. Wang, H. Hao, J. Liu, T. Huang, and A. Yu, "A novel method for preparation of macroposous lithium nickel manganese oxygen as cathode material for lithium ion batteries," *Electrochimica Acta*, vol. 56, no. 11, pp. 4065–4069, Apr. 2011, doi: 10.1016/j.electacta.2010.12.108.

[8] Z. Xie, S. Ellis, W. Xu, D. Dye, J. Zhao, and Y. Wang, "A novel preparation of core–shell electrode materials via evaporation-induced self-assembly of nanoparticles for advanced Li-ion batteries," (Cambridge, England), *Chem. Commun.*, vol. 51, no. 81, pp. 15000–15003, 2015, doi: 10.1039/c5cc05577f.

[9] Y. K. Zeng, T. S. Zhao, X. L. Zhou, L. Zeng, and L. Wei, "The effects of design parameters on the charge-discharge performance of iron-chromium redox flow batteries," *Appl. Energy*, vol. 182, pp. 204–209, Nov. 2016, doi: 10.1016/j.apenergy.2016.08.135.

[10] J. Jiang and H. Ji, "Study of insulation monitoring device for DC system based on multi-switch combination," in *Proc. 2nd Int. Symp. Comput. Intell. Design*, Changsha, China, Dec. 2009, pp. 429–433.

[11] C. Li, S. Luo, C. Cole, and M. Spiryagin, "An overview: Modern techniques for railway vehicle on-board health monitoring systems," *Vehicle Syst. Dyn.*, vol. 55, no. 7, pp. 1045–1070, Jul. 2017, doi: 10.1080/00423114.2017.1296963.

[12] Y.-H. Chiang, W.-Y. Sean, C.-Y. Huang, and L.-H. Chiang Hsieh, "Adaptive control for estimating insulation resistance of high-voltage battery system in electric vehicles," *Environ. Prog. Sustain. Energy*, vol. 36, no. 6, pp. 1882–1887, May 2017, doi: 10.1002/ep.12644.

[13] H. Li, Z. Li, F. Lin, Y. Chen, D. Liu, and B. Wang, "Measurement and analysis of insulation resistance of metallized polypropylene film capacitor under high electric field," in *Proc. IEEE Int. Power Modulator High Voltage Conf. (IPMHVC)*, San Diego, CA, USA, Jun. 2012, pp. 617–619.

[14] H. Torkaman and F. Karimi, "Measurement variations of insulation resistance/polarization index during utilizing time in HV electrical machines—A survey," *Measurement*, vol. 59, pp. 21–29, Jan. 2015, doi: 10.1016/j.measurement.2014.09.034.

[15] E. David, R. Soltani, and L. Lamarre, "PDC measurements to assess machine insulation," *IEEE Trans. Dielectr. Electr. Insul.*, vol. 17, no. 5, pp. 1461–1469, Oct. 2010, doi: 10.1109/TDEI.2010.5595547.

[16] R. Rui and I. Cotton, "Impact of low pressure aerospace environment on machine winding insulation," in *Proc. IEEE Int. Symp. Electr. Insul.*, San Diego, CA, USA, Jun. 2010, pp. 1–5.

[17] B. X. Du and Y. Yamano, "Effects of atmospheric pressure on DC resistance to tracking of polymer insulating materials," *IEEE Trans. Dielectr. Electr. Insul.*, vol. 12, no. 6, pp. 1162–1171, Dec. 2005, doi: 10.1109/TDEI.2005.1561796.

[18] G. Mitic and G. Lefranc, "Localization of electrical-insulation and partial-discharge failures of IGBT modules," *IEEE Trans. Ind. Appl.*, vol. 38, no. 1, pp. 175–180, Jan./Feb. 2002, doi: 10.1109/28.980373.

[19] *Electric Vehicles Safety Requirements*, Standard GB 18384-2020, May 2020.

[20] *Electrically Propelled Road Vehicles-Safety Specifications-Part 3: Electrical Safety*, Standard ISO 6469-3:2018, Oct. 2018.

[21] W. Zhen-Jun and W. Li-Fang, "A novel insulation resistance monitoring device for hybrid electric vehicle," in *Proc. IEEE Vehicle Power Propuls. Conf.*, Harbin, China, Sep. 2008, pp. 1–4.

[22] W. Xuezhe, B. Lu, and S. Zechang, "A method of insulation failure detection on electric vehicle based on FPGA," in *Proc. IEEE Vehicle Power Propuls. Conf.*, Harbin, China, Sep. 2008, pp. 1–5.

[23] C. H. Piao and T. Cong, "Study on isolation monitoring of high-voltage battery system," *Appl. Mech. Mater.*, vols. 44–47, pp. 571–575, Dec. 2010, doi: 10.4028/www.scientific.net/AMM.44-47.571.

[24] J. Li, Z. Wu, Y. Fan, Y. Wang, and J. Jiang, "Research on insulation resistance on-line monitoring for electric vehicle," in *Proc. Int. Conf. Electr. Mach. Syst.*, Nanjing, China, vol. 1, Sep. 2005, pp. 814–817.

[25] J. S. Simons and M. T. Richards, "Non-destructive electrical test methods for evaluating high-voltage stator insulation," *Proc. IEE A, Power Eng.*, vol. 109, no. 3, pp. 71–79, Feb. 2010, doi: 10.1049/pi-a.1962.0013.

[26] A. Mathsyaraja, "Ground fault detection for flexible high voltage power systems," *SAE Int. J. Commercial Vehicles*, vol. 4, no. 1, pp. 185–197, Sep. 2011, doi: 10.4271/2011-01-2252.

[27] J. Tian, Y. Wang, D. Yang, X. Zhang, and Z. Chen, "A real-time insulation detection method for battery packs used in electric vehicles," *J. Power Sources*, vol. 385, pp. 1–9, May 2018, doi: 10.1016/j.jpowsour.2018.03.018.

[28] Y. Wang, C. Zhang, and Z. Chen, "An adaptive remaining energy prediction approach for lithium-ion batteries in electric vehicles," *J. Power Sources*, vol. 305, pp. 80–88, Feb. 2016, doi: 10.1016/j.jpowsour.2015.11.087.

[29] X. Zhang, Y. Wang, C. Liu, and Z. Chen, "A novel approach of remaining discharge energy prediction for large format lithium-ion battery pack," *J. Power Sources*, vol. 343, pp. 216–225, Mar. 2017, doi: 10.1016/j.jpowsour.2017.01.054.

[30] C. Song, Y. Shao, S. Song, S. Peng, F. Zhou, C. Chang, and D. Wang, "Insulation resistance monitoring algorithm for battery pack in electric vehicle based on extended Kalman filtering," *Energies*, vol. 10, no. 5, p. 714, May 2017, doi: 10.3390/en10050714.

[31] X. Cui, Z. Jing, M. Luo, Y. Guo, and H. Qiao, "A new method for state of charge estimation of lithium-ion batteries using square root cubature Kalman filter," *Energies*, vol. 11, no. 1, p. 209, Jan. 2018, doi: 10.3390/en11010209.

[32] X. Cui, Z. He, E. Li, A. Cheng, M. Luo, and Y. Guo, "State-of-charge estimation of power lithium-ion batteries based on an embedded micro control unit using a square root cubature Kalman filter at various ambient temperatures," *Int. J. Energy Res.*, vol. 43, no. 8, pp. 3561–3577, Apr. 2019, doi: 10.1002/er.4503.

[33] M. Beza and M. Bongiorno, "Application of recursive least squares algorithm with variable forgetting factor for frequency component estimation in a generic input signal," *IEEE Trans. Ind. Appl.*, vol. 50, no. 2, pp. 1168–1176, Mar. 2014, doi: 10.1109/TIA.2013.2279195.

[34] X. Wei, M. Yimin, and Z. Feng, "Identification of parameters in Li-ion battery model by least squares method with variable forgetting factor," *Int. J. Comput. Methods*, vol. 17, no. 7, Sep. 2020, Art. no. 1950027, doi: 10.1142/S0219876219500270.

[35] Q. Song, Y. Mi, and W. Lai, "A novel variable forgetting factor recursive least square algorithm to improve the anti-interference ability of battery model parameters identification," *IEEE Access*, vol. 7, pp. 61548–61557, 2019, doi: 10.1109/ACCESS.2019.2903625.

ZHENBIN CHEN was born in 1968. He received the B.E. degree in agricultural mechanization and the M.E. degree in agricultural extension from Hainan University, Haikou, China, in 1990 and 2007, respectively, and the Ph.D. degree in power machinery and engineering from Tongji University, Shanghai, in 2015.

From 1990 to 1996, he worked as an Engineer with the Hainan Agricultural Machinery Research Institute. Since 2004, he has been working as a Lecturer with Hainan University. Since 2015, he has been working as the Vice President of the Mechanical and Electrical Engineering College. In the past five years, he has published more than 20 academic articles and two monographs. His research interests include energy-saving and new energy vehicles, advanced manufacturing and automation, and intelligent connected vehicles. He received the Hainan Provincial Science and Technology Progress Award. He currently serves as a reviewer for several journals, and a reviewer and organizer for national and international conferences.

WEIYA CUI was born in 1995. He received the B.E. degree from the Anyang Institute of Technology, Anyang, China, in 2014. He is currently pursuing the M.E. degree with the Mechanical and Electrical Engineering College, Hainan University, Haikou, China. His research interests include new energy electric vehicles, power battery insulation testing, least squares algorithm, and Kalman filter algorithm.

XIANGYU CUI was born in 1980. He received the M.E. degree in vehicle engineering from the Wuhan University of Technology, Wuhan, China, in 2011, and the Ph.D. degree in vehicle engineering from Hunan University, Changsha, China, in 2019. He is currently a Lecturer with the Key Laboratory of Electrochemical Energy Storage and Energy Conversion of Hainan Province, College of Physics and Electronic Engineering, Hainan Normal University. He has published three articles and holds nine patents. His research interests include power battery modeling and simulation on electric vehicles, design, and control theory of the hybrid power train. He received the first prize for Scientific or Technical Awards from the Haima Automobile Group, in 2011.

HUIMIN QIAO was born in 1983. She received the B.S. degree in automation and the M.S. degree in control theory and control engineering from Jilin University, Changchun, China, in 2005 and 2008, respectively. She is currently pursuing the Ph.D. degree in vehicle engineering with the College of Mechanical and Vehicle Engineering, Hunan University, Changsha, China. Her research on subject with Haima Motor Corporation. Her research interests include automobile software/architecture development innovative subject.

HAO LU was born in 1993. He received the B.E. degree in vehicle engineering from Hainan University, Haikou, China, in 2014, where he is currently pursuing the M.E. degree with the Mechanical and Electrical Engineering College. His research interests include new energy electric vehicles and automotive electronics.

NA QIU received the Ph.D. degree in mechanical engineering from Tongji University. She was a Joint-Ph.D. Student of the University of Florida. She is currently a Lecturer with the Mechanical and Electrical Engineering College, Hainan University, Haikou, China. Her research interests include data mining, artificial intelligence, additive manufacturing, crashworthiness optimization, automotive structure design, optimization and lightweight design.